Supplemental Data Information

Dynamic Transcriptome Analysis Unveils Key Pro-Resolving Factors of Chronic Inflammatory Arthritis

Jin-Sun Kong[1,2,a], Ji-Hwan Park[3,4,a], Seung-Ah Yoo[1], Ki-Myo Kim[1], Yeung-Jin Bae[1], Yune-Jung Park[1,5], Chul-Soo Cho[1,5], Daehee Hwang[3,6,b], and Wan-Uk Kim[1,2,5,b]

[1]Center for Integrative Rheumatoid Transcriptomics and Dynamics, The Catholic University of Korea, Seoul 06591, Republic of Korea

[2]Department of Biomedicine & Health Sciences, The Catholic University of Korea, Seoul 06591, Republic of Korea

[3]Center for Plant Aging Research, Institute for Basic Science (IBS), Daegu 42988, Republic of Korea

[4]Korean Bioinformation Center, Korea Research Institute of Bioscience & Biotechnology, Daejeon 34141, Republic of Korea

[5]Division of Rheumatology, Department of Internal Medicine, The Catholic University of Korea, Seoul 06591, Republic of Korea

[6]Department of Biological Sciences, Seoul National University, Seoul 08826, Republic of Korea

[a]These authors contributed equally to this work.

[b]To whom correspondence should be addressed:
E-mail: wan725@catholic.ac.kr (W. U. Kim) or daehee@snu.ac.kr (D. Hwang)

Short Title: Pro-resolving genes of chronic arthritis

Key Words: Rheumatoid arthritis, Transcriptomes, Resolution dynamics, Pro-resolving genes

This file includes:

Supplemental Notes 1 and 2

Supplemental Materials and Methods

Supplemental Tables 1 to 10

: Supplemental Tables 3, 5, 7, and 8 are provided in additional Excel spreadsheets.

Supplemental Figures 1 to 13

Supplemental References

Supplemental Notes

Supplemental Note 1. Dynamic changes in the expression of resolution-associated genes and activities of immune cells

A number of genes have been reported to be associated with the resolution of inflammation (1, 2). Thus, we investigated the mRNA expression patterns of these genes using gene expression profiles obtained from the microarray experiment. Among them, the following 18 genes involved in the resolution-related processes were up- or down-regulated at the resolution phase of CIA (**Supplemental Figure 1A**): 1) inhibition of neutrophil infiltration (*Mmp12*, *Ccr5*, and *Lgals1*); 2) "Find me" signal (*Cx3cr1* and *Gpr132*); 3) "Eat me" signal (*Ager*, *Axl*, *C1qa*, *Calr*, *Gas6*, *Havcr2*, *Itgav*, and *Mfge8*); 4) clearance of apoptotic neutrophil (*Elmo1* and *Rac1*); and 5) macrophage activation or tissue repair (*Lgals9*, *Tgfb1*, and *Vegfa*). These data indicate that the resolution of inflammation actively occurs during the course of CIA progression.

Several types of cells have been shown to be involved in the resolution of inflammation, including neutrophils, macrophages, T cells, and B cells (1, 2). We next evaluated dynamic changes in the activities of these cells at the induction, peak, and resolution phases by CIBERSORT method (3) using a gene signature matrix of 25 mouse immune cells (4) (**Supplemental Materials and Methods**). The CIBERSORT analysis determined the fractions of 25 immune cells in each synovial tissue sample (**Supplemental Table 1**). These fractions revealed that the subpopulations of T cells ($CD8^+$ memory T cells, $CD4^+$ naïve and follicular T cells, Th1 and Treg cells, and γδ T cells), B cells (naïve B cells and plasma cells), and macrophages (monocytes and M1 and M2 macrophages) were present in the synovial tissue. By comparing the percentages of these cell subpopulations among the induction, peak, and

resolution phases, we found that Treg cells and M2 macrophages were significantly ($p < 0.05$) increased at the resolution phase, compared with the peak and/or induction phases (**Supplemental Figure 1B**). On the other hand, $CD4^+$ naïve T cells were significantly ($p < 0.05$) decreased at the resolution phase while naïve B cells and plasma cells showed no changes and neutrophils were below the detection limit. Consistent with these observations, the median expression levels of T cell marker genes significantly ($p < 0.01$) increased at the resolution phase, whereas those of neutrophil marker genes decreased (**Supplemental Figure 1C**). Relatively insignificant median expression changes of B cell marker genes were observed at the resolution phase. In addition, macrophages showed decreased median expression of marker genes at the peak phase, but this decrease was reduced at the resolution phase, unlike neutrophils (**Supplemental Figure 1C**). The marker genes used are summarized in **Supplemental Table 2**.

Supplemental Note 2. Selection of key regulators for resolution of chronic arthritis

To prioritize key regulators for the resolution of inflammation, we first constructed a network describing interactions among 2836 DEGs using the protein-protein interactomes. In the network model, as key regulator candidates, we identified 85 hub-like molecules that are influential in the network model with significant ($p < 0.05$) degree, betweenness, and closeness centralities (5) (**Supplemental Figure 3A** and **Supplemental Table 7**). Secretory proteins, such as cytokines and chemokines, have been shown to play crucial roles in the suppression or resolution of inflammation (6) and can be utilized as diagnostic and therapeutic targets. We thus selected 16 secretory proteins of 85 hub-like molecules based on the previously reported plasma proteome (7) (**Supplemental Figure 3A**). According to dynamic expression patterns of the 16 key regulator candidates during CIA progression, we focused on the 13 molecules in C3 and C5, which were up-regulated at the resolution phase, including 14-3-3 proteins (*Ywhaq/z*), ribosomal proteins (*Rps3/3a*), heat shock proteins (*Hspa8/d1*, *Tra1* and *Calr*), *H3f3b*, *Rab1*, *Eef2*, *Itgb1*, and *Pabpc1* (**Supplemental Figure 3B**).

Gene expression analysis, as well as functional enrichment analysis of the resolution-associated genes, suggested that suppressive immune cells, T cells and/or macrophages, could play key roles in the resolution of CIA. Thus, among the 13 candidates, we further selected six (*Ywhaz*, *Rps3*, *Hspd1*, *Calr*, *Itgb1*, and *Pabpc1*) anti-inflammatory factors that have been previously shown to be involved in activation of T cells and/or macrophages (**Supplemental Table 8**). Finally, of these six regulators, we selected the following three factors as key regulators of CIA resolution: *Itgb1*, *Rps3* and *Ywhaz*. Ywhaz, also called 14-3-3ζ, interacts with Cbl to modulate PI3K signaling in T cells (8, 9) and also form a complex with Lcp2 to promote the dephosphorylation of TCR signalosome components, such as ZAP70 and PLCγ1, thereby

modulating T cell activation (10) (**Supplemental Figure 2B**). Rps3 modulates the transcriptional regulatory activity of NFκB (11), which plays an important role in the activation of T cells and macrophages (12) (**Supplemental Figure 2B**), and Rps3 fused with cell permeable peptide (PEP-1 peptide) reduces the expression levels of pro-inflammatory cytokines (*Ptgs2*, *Tnf*, *Il1b*, and *Il6*) in mouse ear edema models (13). Itgb1 forms dimers with integrin alphas (e.g., Itga4 and 5) and together these act as co-stimulatory signals that regulate the activities of TCR in T cells (14, 15) (**Supplemental Figure 2B**).

Supplemental Materials and Methods

Evaluation of arthritis scores

Eight mice were used to evaluate arthritis score on a scale of 0 to 4 as described previously (16).

RNA isolation and qRT-PCR analysis

Total RNA was extracted from mouse synovial tissues using RNAzol B (Ambion, Austin, TX) and RNeasy Mini Kit (Qiagen, Hilden, Germany) and then reverse-transcribed into complementary DNA (cDNA) using a reverse transcriptase and a random hexamer (Takara Bio Inc., Shiga, Japan). qRT-PCR (quantitative real-time polymerase chain reaction) was performed in a CFX96 Real-Time PCR System (Bio-Rad, Hercules, CA) using SYBR Green PCR premix (Bio-Rad) according to the manufacturer's instructions. Expression levels of target genes were calculated by the comparative threshold (C_T) method and normalized by those of *Gapdh* (internal control). The primers used for PCR are listed in **Supplemental Table 10**.

Identification of DEGs

Raw data were converted into probe intensities using 'beadarray' package in R software (17), and probe intensities were then normalized using the quantile normalization (18). In order to identify DEGs from each comparison (P/I or R/P), an integrative statistical method was applied to the normalized $\log_2$-probe-intensities as previously described (19). Briefly, for each gene, Student's *t*-test and $\log_2$-median-ratio test were conducted to compute *T* value and $\log_2$-median-ratio between two conditions. Then, empirical null distributions were generated for both *T* values and $\log_2$-median-ratios by performing random permutations of the samples 1,000

times. For each gene, adjusted *p* values from the two tests were calculated by applying two-tailed tests for the measured *T* value and $\log_2$-median-ratio using their corresponding empirical distributions, and the adjusted *p* values from the two tests were combined into an overall *p* value using Stouffer's method (20). For each comparison, the DEGs were identified using the following criteria: the genes with their overall *p* value < 0.05 and the absolute $\log_2$-median-ratio > the mean of 5^{th} and 95^{th} percentiles of the empirical distribution for the $\log_2$-median-ratio.

Deconvolution analysis using CIBERSORT method

We deconvolved cell types from the expression profile from each synovial tissue sample by CIBERSORT method (3) using the gene signature matrix (**B**) of 25 immune cell types provided by Chen *et al*. (4). Briefly, the gene signature matrix was generated through the nu-support vector regression using gene expression profiles of the individual immune cells. For each synovial tissue sample, after enumerating the fractions of the cells (**f**), the method chose a fraction whose product with **B** (**f** × **B**) best explains the intensities (**m**) of genes in the sample. CIBERSORT analysis was conducted with the default option and no quantile normalization. To calculate *p* value, Pearson correlation coefficient between **m** and **f** × **B** was computed. Then, a null empirical distribution of the correlation coefficients was generated by performing random permutations of the mixture matrix (**m**) 100 times, and *p* value was computed by the right-tailed test using the null distribution.

Enrichment analysis of GOBPs

The enrichment analysis was conducted for a list of genes in C1-6 in **Figure 1C** using DAVID software (21). The GOBPs represented by the genes were identified as the ones with *p*

≤ 0.05 and the number of genes > 3. GOBP FAT was used for the analysis of genes in C1-6 (**Supplemental Table 5**). The enrichment *p* value was converted into a *Z*-score by $Z = N^{-1}(1-p)$ for visualization in the heat map, where $N^{-1}(\cdot)$ is the inverse standard normal distribution.

Network analysis

To reconstruct a network model for T cell activation, we first selected a subset of the DEGs that are annotated with T cell differentiation, T cell activation, and TCR signaling pathway. Using the Cytoscape software (22), we visualized interactions among the selected DEGs based on 84,683 protein-protein interactions for 11,649 proteins obtained from the following five interactome databases (**Supplemental Table 6**): the Biological General Repository for Interaction Datasets (BioGRID) (23), the IntAct molecular interaction database (IntAct) (24), the Molecular INTeraction database (MINT) (25), the Database of Interacting Proteins (DIP) (26), and the Interologous Interaction Database (I2D) (27). Once the network model was reconstructed, nodes were arranged based on the information in the KEGG pathway database using Cytoscape software.

Identification of secretory hub-like molecules

We first constructed a resolution-associated network model describing interactions among all DEGs based on the aforementioned protein-protein interactomes. For each DEG, we calculated degree (number of interactors), betweenness, and closeness centralities in the resolution-associated network model as previously described (5). The significance of each centrality measure was computed by the following empirical statistical testing: 1) random sampling of the same number of genes with the DEGs; 2) calculation of the centrality for the randomly sampled genes after reconstructing a network model for them; 3) repetition of steps

1 and 2 1,000 times; 4) generation of an empirical distribution for the resulting centralities from 1,000 random sampling experiments; and 5) for each DEG, computation of p value for the observed centrality by applying the right-tailed test to the empirical distribution. Hub-like molecules were then selected as DEGs with $p < 0.05$ for all three centralities. Finally, among the selected hub-like molecules, we further selected secretory proteins as the ones included in human plasma proteome obtained by liquid chromatography-tandem mass spectrometry (LC-MS/MS) analysis (7). In order to map human proteome into mouse proteome, we used mouse-human orthology in Mouse Genome Information (MGI) database (28).

Immunohistochemistry and immunofluorescence staining

Immunohistochemical staining was done in the paraffin-embedded ankle joints from arthritic mice using anti-Itgb1, anti-Rps3, or anti-Ywhaz (also called anti-14-3-3ζ; Abcam, Cambridge, UK) antibodies as previously described (29). For immunofluorescence experiments, mice were sacrificed at the resolution phase. After hind paw skin was removed using forceps and scissors, the synovial tissues of the ankle were separated from the bone. The tissues were immediately immersed into OCT compound (Sakura Finetek Japan Co.), solidified using liquid nitrogen, and then stored at -70°C until used. Frozen synovial tissues of mice were incubated with anti-CD68 (clone KP1, Abcam), anti-Itgb1 (catalog 179471, Abcam), anti-Rps3 (catalog 77772, Abcam), and anti-Ywhaz (catalog 51129, Abcam) antibodies. The samples were then stained with Alexa Fluor-488- or Fluor-594-conjugated anti-mouse IgG (Invitrogen, Carlsbad, CA) and Prolong Gold Antifade Mount with DAPI, and incubated for 60 minutes at room temperature. Following the incubation, the fluorescence of the sections was detected using a confocal laser scanning microscope (LSM 510 Meta, Zeiss, Oberkochen, Germany).

Western blotting

Synovial tissues of the arthritic mice in addition to macrophages and T cells of the spleen were harvested in RIPA lysis buffer containing protease inhibitors (Roche Diagnostics, Indianapolis, IN) for the Western blot analysis. In some experiments, the protein concentrations of the cell lysates were measured by Bradford protein assay (BioRad). The lysates were boiled in the sample buffer containing β-mercaptoethanol for 5 minutes. The proteins were then subjected to SDS-PAGE and transferred to nitrocellulose membranes. After blocking with 5% skim milk in 0.05% PBS-Tween 20, the membranes were incubated at 4 °C overnight with appropriate dilutions of the following antibodies: polyclonal rabbit anti-Itgb1 (Abcam), polyclonal rabbit anti-Rps3 (Abcam), polyclonal rabbit anti-Ywhaz (Abcam), polyclonal rabbit anti-NOS2 (clone H-174, Santa Cruz Biotechnology, Santa Cruz, CA), polyclonal rabbit anti-Arg1 (clone H-52, Santa Cruz Biotechnology), and anti-β-actin (clone C4, Santa Cruz Biotechnology). The membranes were then visualized using an enhanced chemiluminescent (ECL; Santa Cruz Biotechnology) detection system.

T cell preparation and differentiation in vitro

CD4+ T cells were isolated from the spleens of C57BL6 wild-type mice and purified by a magnetic cell separation (MACS) technique with the CD4+ T-cell isolation beads (Miltenyi Biotec, Bisley, UK) according to the manufacturer's instructions. T cell differentiation was performed as previously described (30). Briefly, CD4+ T cells were cultured with pre-coated anti-CD3 (5 μg/ml, eBioscience, San Diego, CA) and soluble anti-CD28 antibodies (1 μg/ml, eBioscience) in 48 well plates at a concentration of 2×10^5 cells per well in RPMI 1640 medium supplemented with 10 % fetal bovine serum (FBS, ThermoFisher Scientific, Grand Island, NY). The cells were then supplemented with the culture media

containing recombinant cytokines and blocking antibodies as follows: for Th0, recombinant Il2 (10 ng/ml, R&D Systems, Minneapolis, MN); for Th1, recombinant Il2 (10 ng/ml) and Il12 (20 ng/ml, R&D Systems) and anti-Il4 (5 μg/ml, clone 11B11, Biolegend, San Diego, CA); for Th2, recombinant Il2 (10 ng/ml) and Il4 (50 ng/ml, R&D Systems) and anti-Ifng (5 μg/ml, clone R4-6A2, Biolegend) and anti-Il12 antibodies (5 μg/ml, clone C17.8, Biolegend); for Th17, recombinant Il2 (10 ng/ml), Tgfb1 (2 ng/ml, peprotech, Rocky Hill, NJ) and Il6 (20 ng/ml, R&D Systems), and anti-Il4 (5 μg/ml) and anti-Ifng antibodies (5 μg/ml); and for Treg, recombinant Il2 (10 ng/ml) and Tgfb1 (2 ng/ml) and anti-Il4 (5 μg/ml) and anti-Ifng antibodies (5 μg/ml). The stimulated cells were cultured for five days, then gene expression and intracellular molecular production were analyzed.

Isolation and polarization of bone-marrow-derived macrophages

Bone-marrow-derived macrophages were obtained as previously described (31). Briefly, marrow cells were obtained by flushing the femurs and tibias of the C57BL/6 wild type mice. The cells were cultured in RPMI 1640 medium with 10% FBS (ThermoFisher Scientific) and 10 ng/ml of recombinant murine Csf1 (PeproTech) for 7 days. The adherent macrophages were polarized into classical macrophages (M1) or alternative macrophages (M2) by the addition of LPS plus mouse recombinant Ifng or Il4 plus Il13 (10 ng/mL each; R&D Systems) for 48 hours. Polarized macrophages were harvested for FACS analysis, RNA isolation, and Western blotting.

Flow cytometry analysis

Staining of cells was performed at room temperature for 30 minutes using antibodies

against surface molecules including CD4 (clone GK1.5, Biolegend), CD8 (clone 53-6.7, Biolegend), CD19 (clone 1D3, eBioscience), F4/80 (clone BM8, eBioscience), CD80 (clone 16-10A1, eBioscience), CD86 (clone GL-1, eBioscience), CD206 (clone C068C2, eBioscience), and Itgb1 (clone HMb1-1, eBioscience). For intracellular molecule staining, cells were stimulated with PMA (50 ng/ml; Sigma-Aldrich, St. Louis, MO, USA) and ionomycin (1 μg/ml; Sigma-Aldrich) in the presence of GolgiStop™ solution (BD Biosciences, San Jose, CA) for four hours, followed by fixation and permeabilization using Cytofix/Cytoperm™ (BD Biosciences). The cells were then incubated with antibodies against Rps3 (catalog 77772, Abcam) or Ywhaz (catalog 135823, Abcam) for two hours and stained with phycoerythrin (PE)–labeled anti-rabbit IgG antibody. The stained cells were then analyzed using a FACS Canto II system (BD Biosciences) and FlowJo software (TreeStar, Ashland, OR).

Isolation and cell culture of splenocytes, peritoneal macrophages, and mouse FLSs

Splenocytes were obtained from C57BL/6 mice and incubated in RPMI 1640 medium with 10% FBS at 37°C in a 5% CO_2 atmosphere. Peritoneal macrophages were isolated from C57BL/6 mice by injection of 3% thioglycollate into peritoneal cavity for three days, and the cells were then incubated in RPMI 1640 medium with 10% FBS. Mouse fibroblast like synoviocytes (FLSs) were isolated from the joint synovial tissues of mice as previously described (32) and incubated in Dulbecco's modified Eagle's medium (DMEM) with 10% FBS. Splenocytes, peritoneal macrophages, and mouse FLSs were stimulated with multiple doses of recombinant Itgb1, Rps3, or Ywhaz in the absence or presence of LPS, and the cells were then harvested at the indicated times for ELISA and real-time PCR analysis.

Enzyme-linked immunosorbent assay (ELISA)

The protein levels of cytokines (mouse Il6, Tnf, and Il17) in the culture supernatants and YWHAZ in human patient urine samples were measured using ELISA Duo-Set kits (R&D Systems). Itgb1, Rps3 and Ywhaz levels in serum obtained from mice were measured using ELISA kits (MyBioSource, San Diego, CA) according to the manufacturer's instructions.

Isolation and purification of exosomes

Exosomes were isolated from the culture supernatants of differentiated Treg cells by using the Total Exosome Isolation Kit (Invitrogen) according to the manufacturer's protocol. Briefly, supernatants of the cell culture media were collected and centrifuged at 2,000 × g for 30 minutes to eliminate cell debris. The supernatants were mixed with exosome isolation reagents and the mixtures were incubated overnight at 4°C. Next, exosome pellets were collected after centrifugation at 10,000 × g for an hour and then subjected to Western blot analysis using polyclonal rabbit anti-Ywhaz (Abcam), monoclonal rabbit anti-CD63 (clone EPR21151, Abcam), polyclonal rabbit anti-Bcl-2 (clone EPR17509, Abcam), and anti-β-actin (Santa Cruz Biotechnology).

MTT assay

After mouse FLSs or peritoneal macrophages were treated with multiple doses (0, 10, 50, or 100 ng/ml) of recombinant Itgb1, Rps3, or Ywhaz protein for 12 h, the viabilities of the cells were assessed by tetrazolium (MTT) assay as previously described (33).

Transfection of siRNAs for Itgb1, Rps3 and Ywhaz

The siRNAs of *Itgb1*, *Rps3*, and *Ywhaz* and scrambled control siRNA were purchased

from Santa Cruz Biotechnology. Differentiated Treg cells, mouse FLSs, and peritoneal macrophages were transfected with 100 nM of siRNAs using an Amaxa mouse T cell nucleofector kit (Lonza, Cologne, Germany) or Lipofectamine 2000 reagent in Opti-MEM medium (Invitrogen) according to the manufacturer's protocol. After the transfection, the cells were incubated for 4 hours, then the culture medium was replaced with fresh culture medium. Twenty-four hours after transfection, the cells were harvested for further analyses. The efficiencies of *Itgb1*, *Rps3*, and *Ywhaz* siRNAs were determined by qRT-PCR assays.

Assessment of RA activity and treatment response

The disease activity of RA was defined as the disease activity score 28 with erythrocyte sedimentation rate (DAS28-ESR) (34) as low activity at DAS28 ≤ 3.2, moderate activity at 3.2 < DAS28 ≤ 5.1, and high activity DAS28 > 5.1. Four to six months after treatment with biologic or conventional DMARDs, RA patients were further classified into three groups as either good, moderate, or no responders, according to European League Against Rheumatism (EULAR) response categories (35).

Generation of adenoviral vector bearing Ywhaz gene

Adenoviral vector containing *Ywhaz* (Ad-*Ywhaz*) or the empty adenovirus control vector (Ad-Con) was purchased from SIRION Biotech GmbH. Briefly, plasmids containing *Ywhaz* (CMV-*Ywhaz*-IRES-*GFP*) or empty vector (CMV-*GFP*) were transferred to *E. coli* cells carrying a BAC vector, which contains the genome of a replication-deficient Ad5-based vector lacking E1/E3 genes. After the recombination of the plasmids and the BAC vector, the recombinant viral DNA (Ad5-CMV-*Ywhaz*-IRES-*GFP* or Ad5-CMV-*GFP*) was obtained by screening of *E.coli* colonies and digestion of BAC-DNA with Pac I restriction enzyme. The

adenoviral DNA was transfected into HEK-293 cells for amplification, and high-titer recombinant adenoviruses were prepared by purification according to the established method.

Effect of Ad-Ywhaz on arthritis progression

In order to test the effect of *Ywhaz* overexpression on chronic arthritis, 1×10^8 plaque-forming units (PFU) of Ad-*Ywhaz* tagged with *GFP* or Ad-Con (in 10 μl HEPES) were injected into the ankle joints of the mice 30 and 37 days after the primary immunization. Synovial tissues were isolated from the ankle joints to measure the gene and protein expression levels of Ywhaz and pro-inflammatory cytokines (Il6 and Tnf) and to perform histologic analysis as previously described (16). The severity degrees of inflammation, synovial hyperplasia, and bone destruction in the joints were determined using a standard scoring protocol, in which each of the three severities was scored based on a scale of 0–4, where 0=absent, 1=weak, 2=moderate, 3=severe, and 4=very severe. In order to compare the production of pro-inflammatory cytokines in lymph node cells and splenocytes of CIA mice injected with Ad-*Ywhaz* or ad-Con, the cells were obtained from each group of mice at 33 (n=4) and 52 days (n=6) after the primary immunization, then stimulated them with LPS (10 ng/ml) or anti-CD3 (1 μg/ml) plus anti-CD28 antibodies (1 μg/ml). The levels of cytokines in cell culture supernatants were measured by ELISA.

To test whether Ywhaz effect on CIA is dependent on the 14-amino acid sequence (SVTEQGAELSNEER) of Ywhaz, named PEPITEM, which is known to affect trans-endothelial migration of T cells (36), we intra-articularly or intra-peritoneally injected the PEPITEM (100 μg) or a control peptide (100 μg) with the scrambled sequence of PEPITEM twice a week over 3 weeks into mice with pre-clinical CIA 21 days after the primary immunization.

Imaging of GFP

For GFP imaging, 1×10^8 plaque-forming units (PFU) of Ad-*Ywhaz* tagged with *GFP* (Ad5-CMV-*Ywhaz*-IRES-*GFP*) was injected intra-articularly into the ankle joint (10 μl) or intravenously (100 μl) into the tail vein of CIA mice at 30 days after the primary immunization. The mice were sacrificed at 24, 48 and 72 hours after the injection and the lung, liver, and ankle joints of the mice were harvested. GFP fluorescence was visualized by using the IVIS Lumina XRMS imaging system (PerkinElmer, Hopkinton, MA) with the standard filter set for GFP. Radiant efficiency in the region of interest was calculated as fluorescence emission radiance (photons sec^{-1} cm^{-2} $steradian^{-1}$) per incident excitation irradiance (μW cm^{-2}) by using Living Image software (PerkinElmer).

Assay for IgG antibodies against CII

Sera were collected from each group of mice 52 days after primary immunization and stored at –20 °C until the experiments. IgG anti-CII levels in the sera were determined using a commercially available ELISA kit (Chondrex) as previously described (16).

Batch effect correction for multiple comparisons

For multiple comparisons of qRT-PCR, ELISA, Western blotting, and flow cytometry data obtained from more than two conditions (e.g., doses or cell subtypes), we performed a normalization between experimental batches as follows. For each dataset (e.g., qRT-PCR dataset), we first calculated means (m_1, m_2, …, m_k) and standard deviations (s_1, s_2, …, s_k) for individual batches (k). The pooled standard deviation (s_p) and mean (m_p) for all batches were computed using the following equations: $m_p = \frac{\sum_{i=1}^{k} n_i m_i}{\sum_{i=1}^{k} n_i}$ and $s_p = \sqrt{\frac{\sum_{i=1}^{k}(n_i-1)s_i^2}{\sum_{i=1}^{k}(n_i-1)}}$, where n_i

denotes the number of conditions in batch *i* (37). For each batch, the original values were then adjusted to have the s_p and m_p across multiple conditions. These adjusted values were used for both visualization and multiple comparison tests (one-way ANOVA with a default post hoc test in GraphPad Prism, Tukey's or Dunnett's correction).

Supplemental Tables

Supplemental Table 1. Comparisons of 25 immune cell fractions at the three phases. For each immune cell present in the synovial tissue, the mean and standard deviation (SD) of its fractions (%) at the induction (I), peak (P), and resolution (R) phases are shown with *p* values of all possible comparisons among the three phases (P/I, R/I, and R/P). Red color represents $p < 0.05$ by one-way ANOVA with a post-hoc test (Tukey's correction).

Immune cell type	Presence in synovial tissue	Mean ± SD (%)			*p* values		
		I	P	R	P/I	R/I	R/P
Mast Cells	--	--	--	--	--	--	--
Neutrophil Cells	--	--	--	--	--	--	--
Eosinophil Cells	Present	0.36 ± 0.15	0.31 ± 0.10	0.22 ± 0.04	0.883	0.499	0.738
B Cells Memory	--	--	--	--	--	--	--
B Cells Naive	Present	22.58 ± 0.24	16.31 ± 0.37	22.25 ± 4.52	0.184	0.991	0.205
Plasma Cells	Present	31.22 ± 0.57	21.95 ± 0.60	26.24 ± 6.46	0.174	0.475	0.558
Monocyte	Present	1.07 ± 0.03	1.10 ± 0.12	1.44 ± 0.69	0.997	0.681	0.719
M0 Macrophage	--	--	--	--	--	--	--
M1 Macrophage	Present	1.39 ± 0.45	0.87 ± 0.19	0.81 ± 0.43	0.448	0.383	0.984
M2 Macrophage	Present	4.49 ± 0.23	4.58 ± 0.50	8.00 ± 0.23	0.964	0.004	0.005
DC Actived	--	--	--	--	--	--	--
DC Immature	Present	1.28 ± 0.10	1.13 ± 0.23	0.59 ± 0.84	0.954	0.464	0.598
T Cells CD8 Actived	--	--	--	--	--	--	--

T Cells CD8 Memory	Present	0.94 ± 1.31	1.20 ± 0.21	0.99 ± 0.79	0.955	0.999	0.969
T Cells CD8 Naive	--	--	--	--	--	--	--
T Cells CD4 Memory	--	--	--	--	--	--	--
T Cells CD4 Naive	Present	18.54 ± 0.26	24.05 ± 1.87	13.96 ± 2.37	0.101	0.152	0.021
T Cells CD4 Follicular	Present	6.92 ± 0.31	11.11 ± 1.69	7.65 ± 0.34	0.051	0.767	0.082
Th1 Cells	Present	1.30 ± 0.12	2.24 ± 0.73	2.11 ± 1.11	0.522	0.602	0.985
Th2 Cells	--	--	--	--	--	--	--
Th17 Cells	--	--	--	--	--	--	--
Treg Cells	Present	2.23 ± 1.00	0.26 ± 0.37	3.11 ± 0.42	0.115	0.467	0.046
GammaDelta T Cells	Present	3.15 ± 0.03	3.84 ± 0.41	2.97 ± 1.55	0.758	0.979	0.656
NK Resting	Present	4.00 ± 1.72	2.42 ± 0.42	4.81 ± 1.80	0.585	0.850	0.357
NK.Actived	Present	0.45 ± 0.63	5.02 ± 1.37	0 ± 0	0.027	0.871	0.021

Supplemental Table 2. Marker genes of T and B cells, neutrophils, and macrophages. For each marker gene, Entrez ID and $\log_2$-intensities at the three phases, induction (I), Peak (P), and resolution (R) phase are shown. For the T helper (Th) cell marker genes, subtypes are denoted by superscripts on gene symbols (†Th1, ‡Th17, and §Treg).

	Entrez ID	Symbol	I	P	R	References
T-cell marker genes	12500	*Cd3d*	12.15	12.45	12.14	(38)
	12501	*Cd3e*	11.56	12.27	11.81	(38)
	12502	*Cd3g*	12.56	13.07	13.11	(38)
	12511	*Cd6*	11.15	11.54	11.12	(38)
	80901	*Cxcr6*†	6.94	7.05	7.51	(39, 40)
	15978	*Ifng*†	7.26	7.55	7.83	(39, 40)
	16182	*Il18r1*†	9.79	9.62	10.22	(41)
	16174	*Il18rap*†	7.18	7.24	7.57	(39, 40)
	57765	*Tbx21*†	7.47	7.46	7.51	(39, 40)
	16171	*Il17a*‡	6.93	6.91	7.08	(39, 40, 42)
	19883	*Rora*‡	7.75	7.69	8.14	(39, 40, 42)
	12774	*Ccr5*§	8.20	8.69	9.37	(43)
	12487	*Cd28*§	8.69	8.57	8.91	(44)
	12477	*Ctla4*§	8.24	8.12	8.60	(45)
	20371	*Foxp3*§	8.75	9.10	8.94	(46)
	54167	*Icos*§	7.88	7.78	8.29	(47)
	16407	*Itgae*§	9.79	9.84	10.17	(48)
B-cell marker genes	12478	*Cd19*	10.64	10.32	10.84	(49)
	12483	*Cd22*	7.62	6.78	7.73	(50)
	21939	*Cd40*	12.06	11.98	11.90	(51)

	12518	*Cd79a*	12.53	12.33	12.69	(52)
	15985	*Cd79b*	13.48	13.57	13.36	(52)
	12902	*Cr2*	7.72	7.88	7.76	(49)
	12482	*Ms4a1*	9.15	8.86	9.35	(53)
Neutrophil marker genes	14131	*Fcgr3*	9.31	8.78	8.64	(54)
	16819	*Lcn2*	8.65	8.40	7.88	(55)
	17002	*Ltf*	9.13	8.57	7.73	(56)
	20202	*S100a9*	10.09	9.55	9.41	(57)
Macrophage marker genes	12514	*Cd68*	8.83	8.74	8.18	(58)
	12524	*Cd86*	10.84	10.51	10.31	(59)
	13038	*Ctsk*	7.64	7.26	7.19	(60)
	17289	*Mertk*	7.78	7.40	7.30	(61)
	17533	*Mrc1*	8.63	7.93	7.88	(62)
	57262	*Retnla*	7.65	7.26	7.05	(62)
	24088	*Tlr2*	9.21	9.01	9.01	(63)
	20307	*Ccl8*	10.32	9.21	9.84	(64)
	12475	*Cd14*	8.39	7.88	8.06	(65)
	12978	*Csf1r*	8.77	8.22	8.25	(66)
	17329	*Cxcl9*	11.87	11.24	11.93	(67)
	77125	*Il33*	8.35	7.88	8.32	(68)
	16600	*Klf4*	6.79	6.98	7.82	(69)
	17105	*Lyz2*	11.83	10.87	11.58	(70)

Supplemental Table 3. Differentially expressed genes (DEGs) from the comparisons of P/I and R/P. For each DEG, whether the DEG was up- (Up) or down-regulated (Down) in the two comparisons is shown, together with its $\log_2$-fold-changes and overall *p* values. For the DEG, Entrez ID, gene name, description, and clusters to which they belonged are also shown.

See the attached excel file named “Supplemental Table 3.xlsx”.

Supplemental Table 4. Clusters of DEGs based on their differential expression patterns in the two comparisons of peak versus induction phase (P/I) and resolution versus peak phase (R/P). Colors represent up- (U; red) and down-regulated genes (D; blue) in the comparison. C1-6 were used for functional enrichment analysis of gene ontology biological processes, since C7 and C8 only included 12 up-regulated and 10 down-regulated genes, respectively.

Cluster	P/I	R/P	Number of DEGs
1	U	-	456
2	U	D	399
3	-	U	499
4	-	D	542
5	D	U	419
6	D	-	499
7	U	U	12
8	D	D	10

Supplemental Table 5. GOBPs enriched by the DEGs in the six clusters. For each cluster (C1-6), GOBPs significantly ($p \leq 0.05$ and number of genes > 3) enriched by the DEGs in the cluster are shown, together with the numbers of DEGs involved in the corresponding GOBPs (Count) and the enrichment *p* values.

See the attached excel file named “Supplemental Table 5.xlsx”.

Supplemental Table 6. Protein-protein interactions obtained from five public interactome databases. These interactions between 11,649 proteins are used for network analysis.

	BioGRID	IntAct	MINT	DIP	I2D	Total
Number of Interactions	3,899	4,842	1,278	431	78,057	84,683
Number of Proteins	2,214	2,868	1,230	513	11,034	11,649

Supplemental Table 7. Key regulator candidates identified from a resolution-associated network model. For each of the 85 hub-like molecules, Entrez ID, gene name, description, and cluster to which it belongs are shown together with its degree, betweenness, and closeness centralities, as well as the significance of the individual centralities (*p* value) in the resolution-associated network. In addition, differential expression patterns of the molecules in P/I and R/P ("Up" or "Down") and secretory proteins reported previously in the plasma proteome ("secreted") are shown.

See the attached excel file named "Supplemental Table 7.xlsx".

Supplemental Table 8. Association of the 13 secretory hub-like molecules with activation of T cells and/or macrophages and anti-inflammation. For each regulator, Entrez ID, gene name, description, and cluster to which it belongs are shown in the table. The previously reported associations with activation of the cells and anti-inflammatory functions are described together with the references.

See the attached excel file named “Supplemental Table 8.xlsx”.

Supplemental Table 9. Clinical characteristics of patients with rheumatoid arthritis.

Variables	Rheumatoid arthritis (N=65)
Age, year	57.2 ± 10.3
Body mass index, kg/m^2	22.8 ± 3.1
Disease duration, year	8.7 ± 8.6
Diabetes mellitus, yes	3 (4.6%)
Coronary artery disease, yes	1 (1.5%)
Hypertension, yes	12 (18.5%)
Smoking, yes	1 (1.5%)
White blood cells, $x10^9/L$	7396.5 ± 2731.8
Hemoglobin, mg/dL	12.6 ± 1.4
Platelet, $x10^9/L$	260.8 ± 70.8
Creatinine, mg/dL	0.7 ± 0.2
Total protein, mg/dL	6.9 ± 0.5
Albumin, mg/dL	3.9 ± 0.5
Erythrocyte sedimentation rate, mm/hour	36.5 ± 23.9
C-reactive protein, mg/dL	1.1 ± 1.9
Rheumatoid factor, positivity	56 (86.2%)
Anti-cyclic citrullinated peptide antibody, positivity (n=54)	46 (85.2%)
Urine creatinine, mg/dL	107.2 ± 77.2
Urine protein, mg/dL	8.0 ± 22.3
Disease Activity Score of 28 joints	4.2 ± 1.2
Tender joints count	3.2 ± 4.2
Swollen joints count	2.2 ± 3.9
Modified Sharp score	35.3 ± 46.2
Joints space narrowing score	21.3 ± 25.8
Joints erosion score	14.0 ± 22.4
Prednisolone, yes	52 (81.2%)
Methotrexate, yes	48 (73.8%)
Hydroxychloroquine, yes	32 (50.0%)
Bucillamine, yes	4 (6.2%)
Sulfasalazine, yes	7 (10.9%)
Leflunomide, yes	26 (40.6%)
Anti-tumor necrosis factor alpha inhibitors, yes	8 (12.3%)
Tacrolimus, yes	14 (22.2%)
Statin, yes	8 (12.3%)

Supplemental Table 10. Primers used for qRT-PCR assays.

Name	Forward primers	Reverse primers
Arg1	5′-CTCCAAGCCAAAGTCCTTAGAG-3′	5′-AGGAGCTGTCATTAGGGACATC-3′
Foxp3	5′-GGCCCTTCTCCAGGACAGA-3′	5′-GCTGATCATGGCTGGGTTGT-3′
Gapdh	5′-AGGTCGGTGTGAACGGATTTG-3′	5′-TGTAGACCATGTAGTTGAGGTCA-3′
Gata3	5′-GGAAACTCCGTCAGGGCTA-3′	5′-AGAGATCCGTGCAGCAGAG-3′
Il10	5′-GGGTTGCCAAGCCTTATGG-3′	5′-AGCCGCATCCTGAGGGTCTT-3′
Il1b	5′-GTGGCTGTGGAGAAGCTGTG-3′	5′-GAAGGTCCACGGGAAAGACAC-3′
Il4	5′-CCTCACAGCAACGAAGAACA-3′	5′-TGGACTCATTCATGGTGCAG-3′
Il6	5′-TTCCATCCAGTTGCCTTCTTG-3′	5′-AGGTCTGTTGGGAGTGGTATC-3′
Il8	5′-CCATGGGTGAAGGCTACTGT-3′	5′-TGTTCTCAGGTCTCCCAAATG-3′
Itgb1	5′-GGACAGGAGAAAATGGACGA-3′	5′-TCAGTGAAGCCCAGAGGTTT-3′
Nos2	5′-GTTCTCAGCCCAACAATACAAGA-3′	5′-GTGGACGGGTCGATGTCAC-3′
Ptgs2	5′-AACCGCATTGCCTCTGAAT-3′	5′-CATGTTCCAGGAGGATGGAG-3′
Rorc	5′-TGAGGAAACCAGGCATCCTGAACT-3′	5′-ACTCCACCACATACTGAATGGCC-3′
Rps3	5′-GAGAAAGTGGCCACAAGAGG-3′	5′-CTTCCCAGACACCACAACCT-3′
Tbx21	5′-TTCCCATTCCTGTCCTTCAC-3′	5′-CCACATCCACAAACATCCTG-3′
Tgfb1	5′-CTCCCGTGGCTTCTAGTGC-3′	5′-GCCTTAGTTTGGACAGGATCTG-3′
Tnf	5′-TGAAGG GAATGGGTGTTCAT-3′	5′-TTGGACCCTGAGCCATAATC-3′
Ywhaz	5′-TTGAGCAGAAGACGGAAGGT-3′	5′-GAAGCATTGGGGATCAAGAA-3′

Supplemental Figures

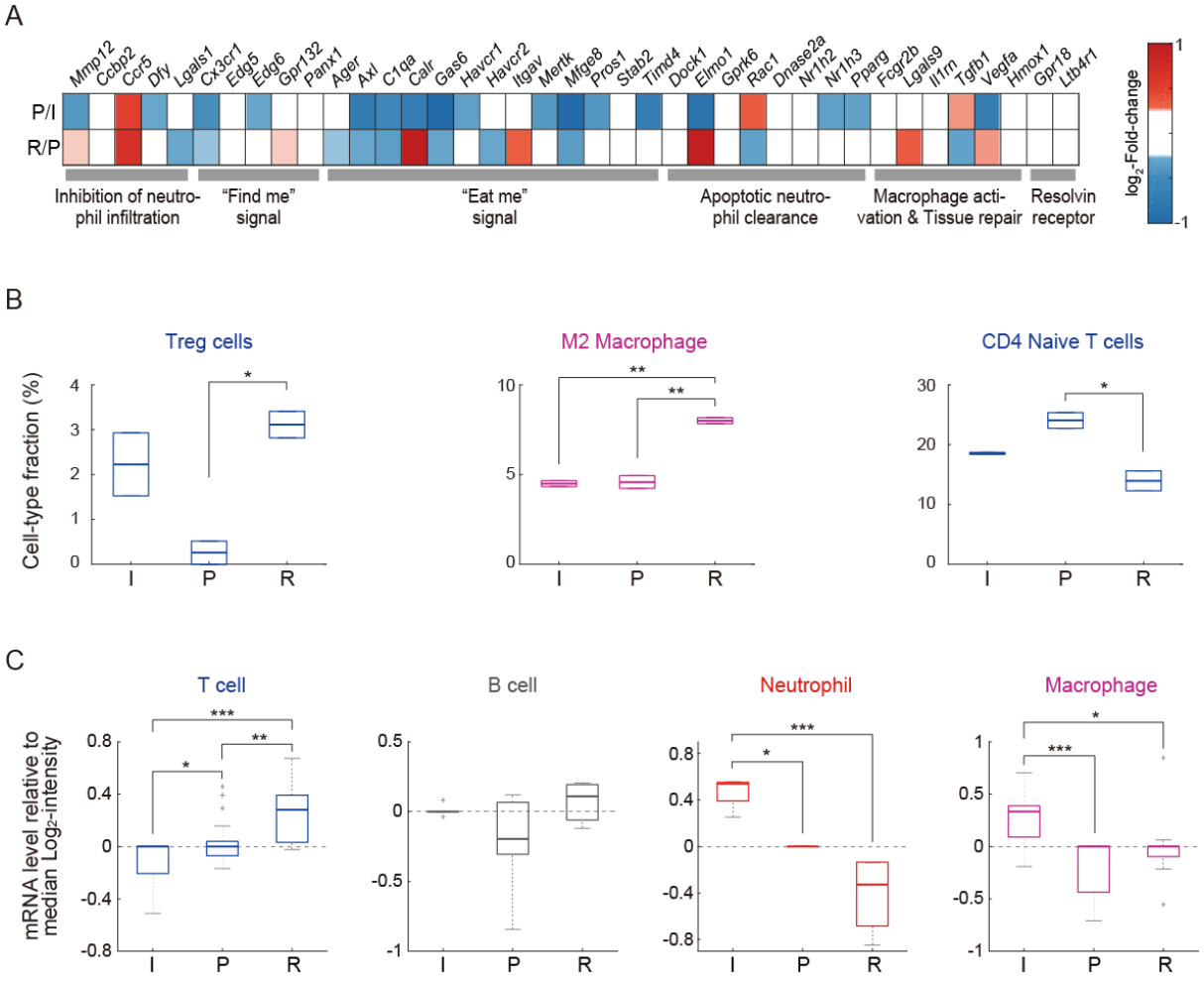

Supplemental Figure 1. Dynamic changes in the expression of resolution-associated genes and immune cell subpopulations. (**A**) Dynamic expression changes of genes involved in the indicated cellular processes associated with resolution of inflammation. Colors indicate up- (red) and down-regulation (blue) of genes in the comparisons of peak versus induction phase (P/I) and resolution versus peak phase (R/P). Color bars represent the gradients of $\log_2$-fold-changes in P/I or R/P. (**B**) Fractions of immune cell subpopulations at the three phases estimated by CIBERSORT method. (**C**) Distribution of mRNA levels of marker genes for the indicated cell types at I, P, and R phases. For each marker gene, relative mRNA levels at the three phases are calculated as its $\log_2$-intensities normalized by the median $\log_2$-intensity across the three phases. Normalized relative mRNA levels are displayed in box plots. The boxes display the lower, median, and upper quartiles; the whiskers represent the minimum and maximum values (**B** and **C**). *$p < 0.05$, **$p < 0.01$, and ***$p < 0.001$ by one-way ANOVA with a post-hoc test (Tukey's correction).

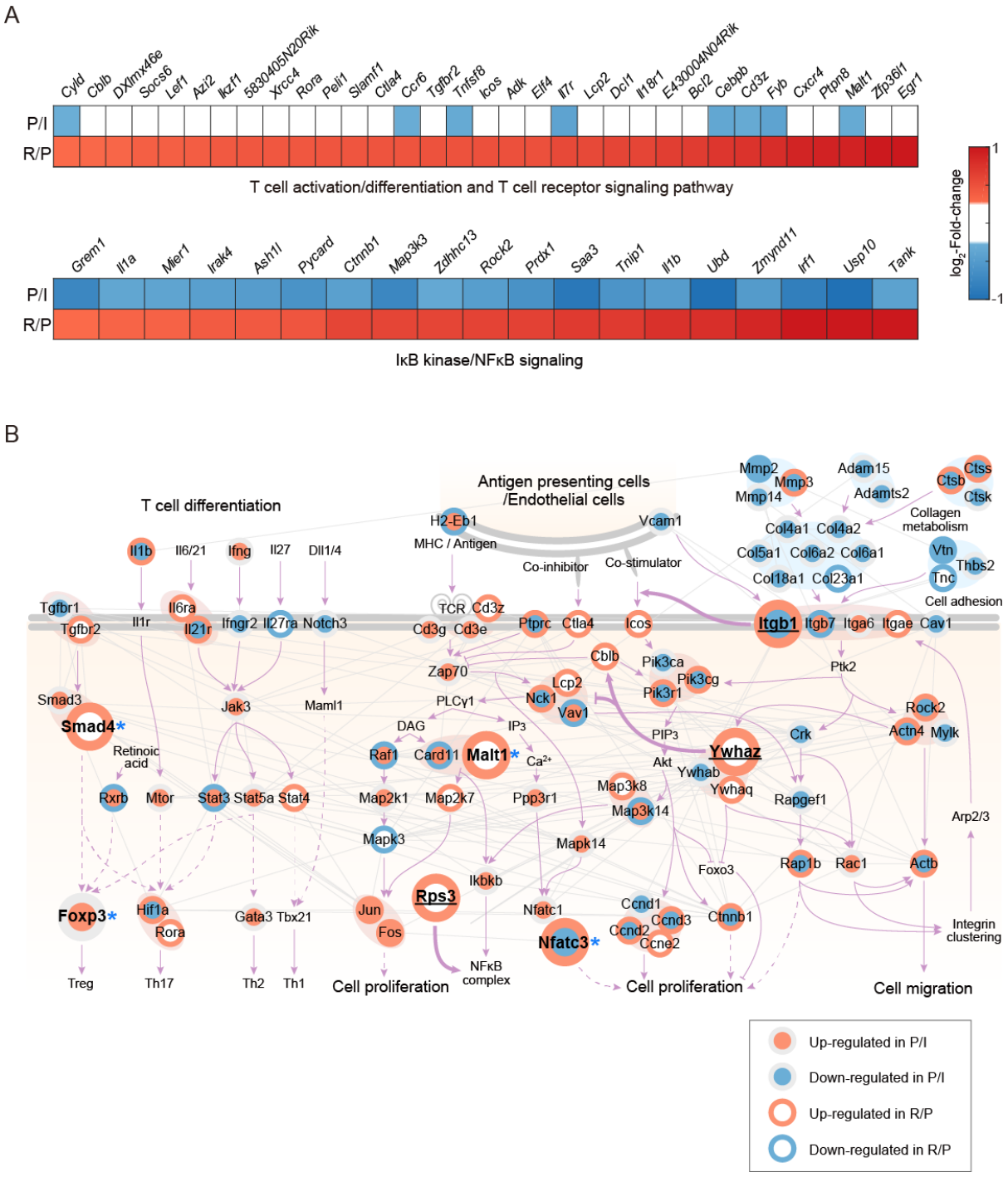

Supplemental Figure 2. T cell differentiation/activation and macrophage activation represented by DEGs. (**A**) Up-regulated genes during the resolution in C3 and C5, which are involved in T cell functions (T cell activation and differentiation and T cell receptor signaling pathway in the top heat map) and macrophage functions (IκB kinase/NFκB signaling in the bottom heat map). Colors indicate up- (red) and down-regulation (blue) of genes in the two

comparisons, peak versus induction phase (P/I) and resolution versus peak phase (R/P). The color bar represents the gradient of log_2-fold-changes in P/I or R/P. (**B**) Network model describing interactions among DEGs involved in T cell differentiation and activation and TCR signaling. Based on KEGG pathway database and literature, pathway information (activation and suppression) is added to the network models. Center and boundary colors of nodes represent up- (orange) or down-regulation (blue) in the comparisons of the peak versus induction phase (P/I) and the resolution versus peak phase (R/P), respectively. The gray solid lines represent protein-protein interactions, and the *arrows* and *inhibition* symbols denote activation and suppression, respectively. Among the arrows, the dashed lines indicate transcriptional regulatory relationships. Large nodes with asterisks and the ones with underline symbols are the genes examined by qRT-PCR in **Figure 1E** and the key regulators selected in **Supplemental Figure 3B**, respectively. In TGFβ signaling, *Tgfbr2*, *Smad4*, and *Rora* were up-regulated at the R phase. In JAK-STAT signaling, ligands/receptors (*Il1b*, *Il6ra*, and *Il21ra*), signaling molecules (*Jak3*), and transcription factors (TFs; *Stat3/4/5a*, *Foxp3*, *Gata3*, and *Rora*) were up-regulated at the P or R phase. In TCR signaling, co-receptors and regulators (*Cd3e/g/z*, *Ctla4*, and *Icos*), signaling molecules (*Zap70*, *Cblb*, *Raf1*, *Card11*, *Malt1*, *Map2k1/7*, and *Mapk14*), and TFs (*Jun*, *Fos*, and *Nfatc1/3*) were similarly up-regulated. However, in actin cytoskeletal signaling, collagens, extracellular proteases (*Mmp2/3/14* and *Adam15/ts2*), and signaling molecules were down-regulated at the P phase, but many (*Itgae/b1*, *Rock2*, *Actn4*, *Pik3r1/cg*, *Rap1b*, *Ccnd2/d3/e2*, *Ctnnb1*, and *Actb*) were up-regulated at the R phase.

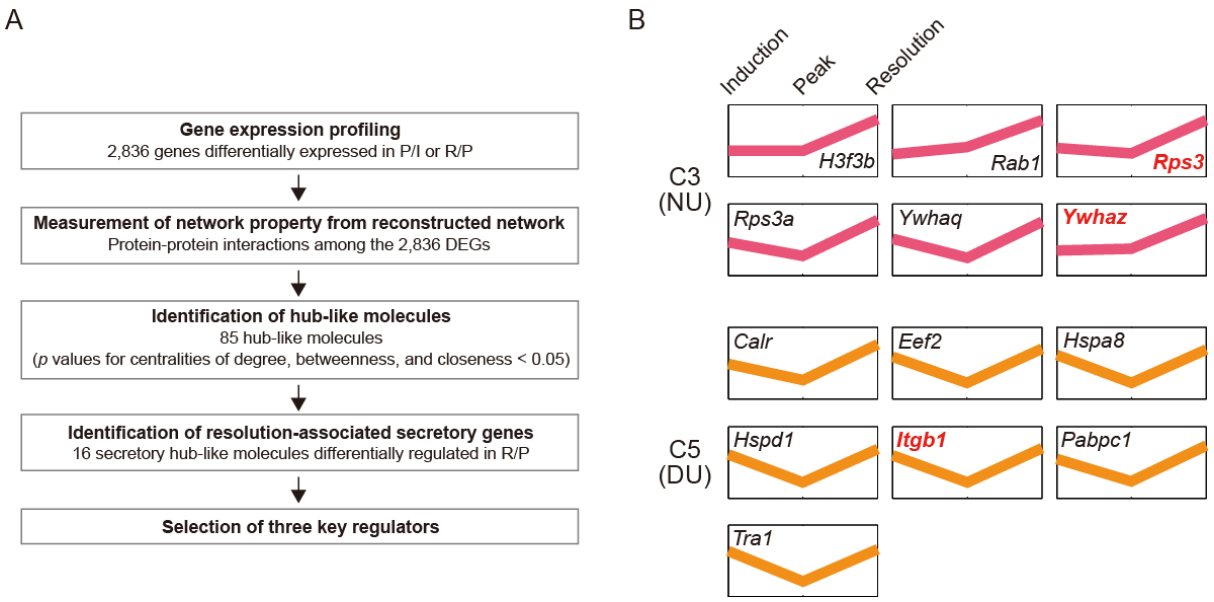

Supplemental Figure 3. Selection of key regulators of resolution of CIA. (**A**) An overall scheme for selecting potential key regulators of CIA resolution. (**B**) Dynamic expression patterns of 13 key regulator candidates. Mean expression levels at induction, peak, and resolution phases are shown. Different colors are used to distinguish the candidates in different clusters. NU (for C3) indicates no expression change at the peak phase and upregulation at the resolution phase. DU (for C5) indicates downregulation at the peak phase and upregulation at the resolution phase.

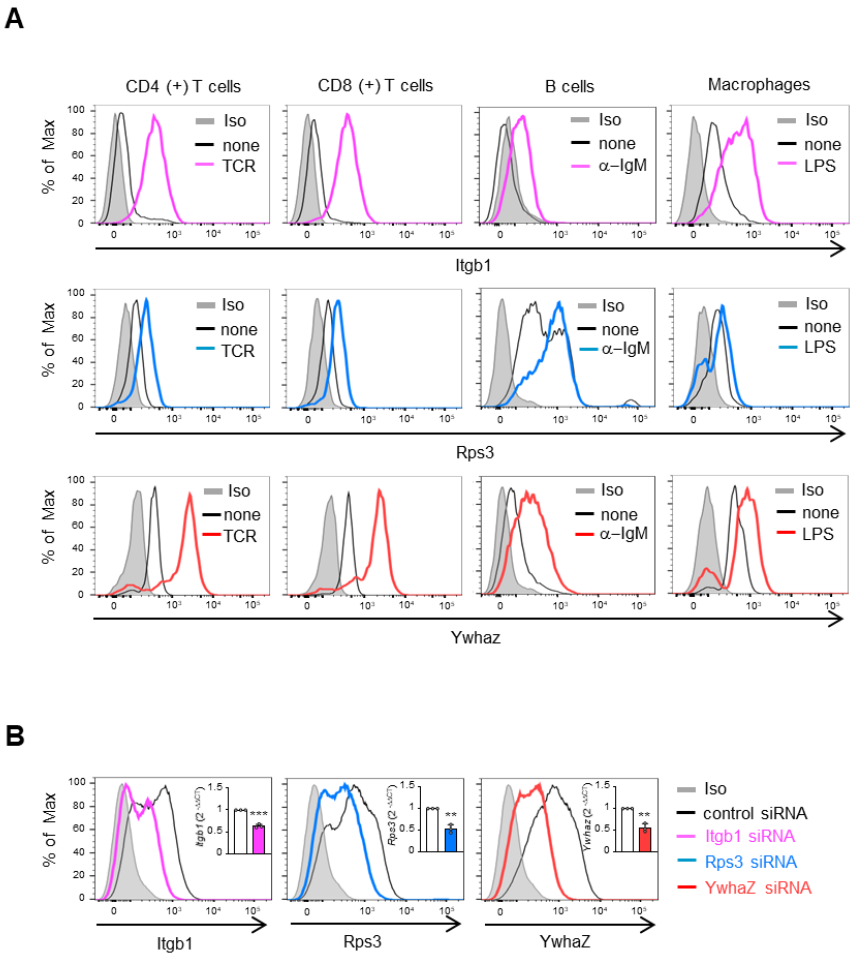

Supplemental Figure 4. Expression of three key regulators in activated T cells, B cells, and macrophages. (**A**) Expression of Itgb1, Rps3, and Ywhaz in T cells, B cells, and macrophages. Mouse splenocytes were isolated and stimulated with anti-CD3 (1 μg/ml) and anti-CD28 (1 μg/ml) antibodies for 24 hours, anti-IgM antibodies (α-IgM, 10 ng/ml) for 48 hours, or LPS (10 ng/ml) for 24 hours. The cells were then subjected to flow cytometry analysis using antibodies against CD4, CD8, CD19, or F4/80, and antibodies against ltgb1, Rps3, and Ywhaz. Gray-shaded regions and black lines in the histograms indicate isotype control (Iso) and unstimulated splenocytes, respectively, while the pink, blue, and red lines represent splenocytes expressing Itgb1, Rps3, and Ywhaz, respectively, in the above stimulation conditions. (**B**) Evaluation of the specificity of anti-Itgb1, anti-Rps3, and anti-Ywhaz antibodies used for flow cytometry. $CD4^+$ T cells isolated from mouse splenocytes were stimulated with anti-CD3 plus anti-CD28 (1 μg/ml) antibodies for 24 hours and treated with Itgb1 (pink), Rps3 (blue), Ywhaz (red), or control siRNAs (black) for 24 hours. The histograms show the representative results from three independent experiments with similar results. The mRNA expression levels of Itgb1, Rps3 or Ywhaz in the transfected cells with each siRNA were simultaneously measured by qRT-PCR analysis and are shown in the insert. Data are the mean ± SEM (n=3). $^{**}p < 0.01$ and $^{***}p < 0.001$ by Student's *t* test.

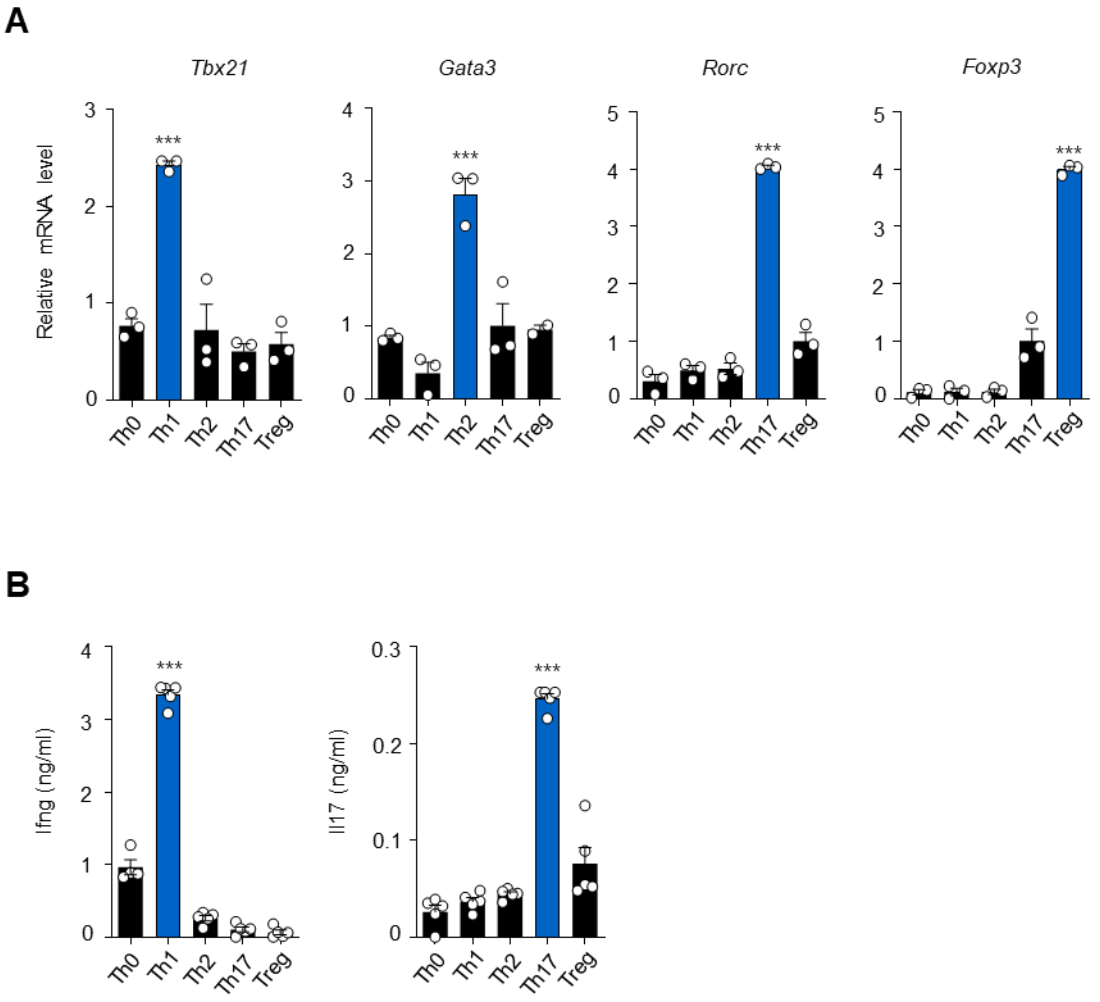

Supplemental Figure 5. Validation of Th cell differentiation to Th1, Th2, Th17 or Treg cells. (**A**) mRNA expression levels of *Tbx21*, *Gata3*, *Rorc*, and *Foxp3* (transcription factors specific to Th1, Th2, Th17, and Treg, respectively) in $CD4^+$ Th cells, which were measured by qRT-PCR under Th1, Th2, Th17, and Treg-polarizing conditions (n=3). mRNA expression levels are normalized by that of *Gapdh* (internal control). (**B**) Levels of Ifng and Il17 in the culture supernatants of unpolarized Th0, Th1, Th2, Th17, or Treg cells, which were determined by ELISA assays (n=4 to 5). Data are the mean ± SEM. ***$p < 0.001$ by one-way analysis of variance (ANOVA) with a post-hoc test (Tukey's correction).

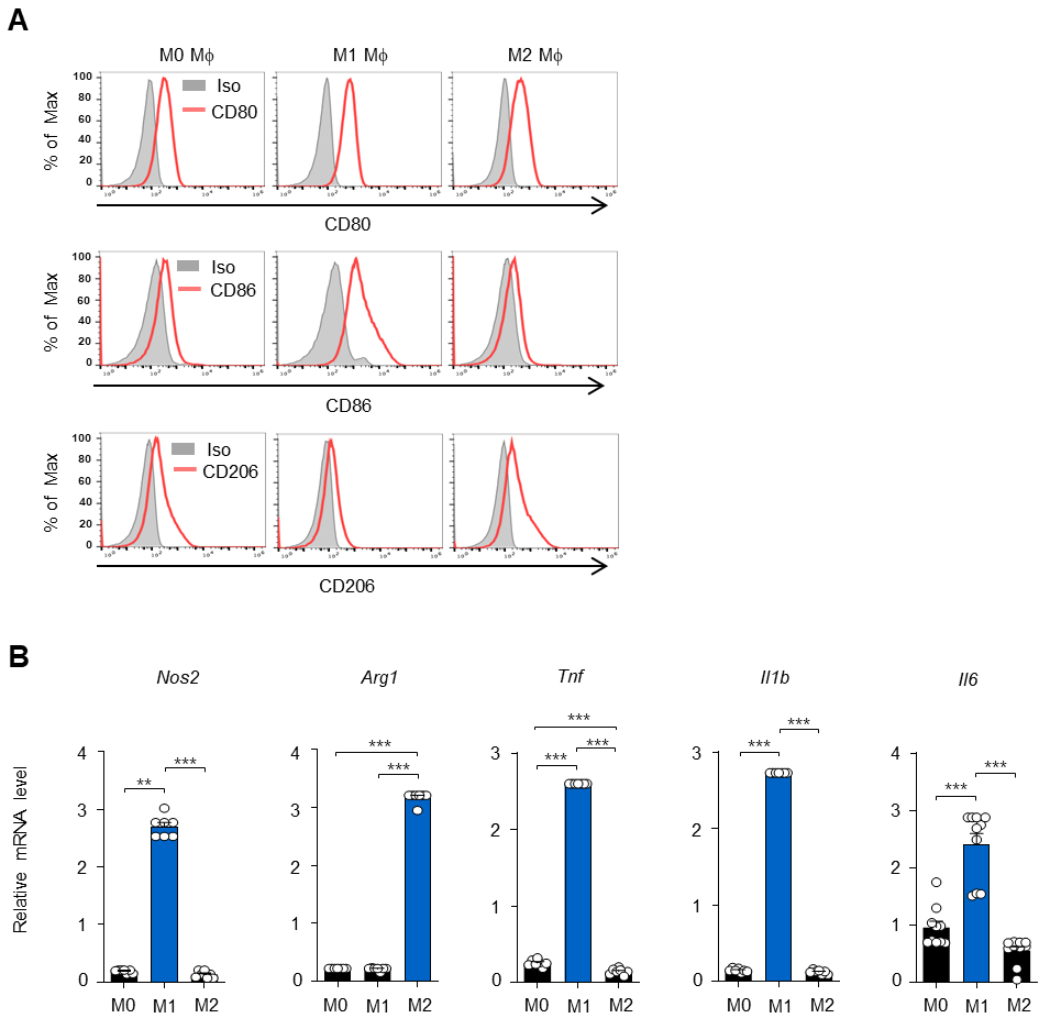

Supplemental Figure 6. Validation of polarized macrophages derived from bone marrow. (**A**) Confirmation of mature macrophages derived from bone marrow and their polarized descendants (M1 and M2) by flow cytometry analysis. The cells were initially gated on CD11b and F4/80, and then the expression of surface markers (CD80, CD86, and CD206) in the cells was assessed. Data are representative of three independent experiments with similar results, presented in the overlap histograms. Gray-shaded regions and red lines in the histograms indicate isotype control and the macrophages expressing CD80, CD86, and CD206, respectively. (**B**) mRNA expression levels of marker genes for M1 (*Nos2, Tnf, Il1b*, and *Il6*) and M2 macrophages (*Arg1*) measured by qRT-PCR assays. mRNA expression levels are first normalized by those of *Gapdh* (internal control) and then further normalized by the mean mRNA expression level in the M0 macrophages. Data are the mean ± SEM (n=7). $^{**}p < 0.01$ and $^{***}p < 0.001$ as determined by one-way ANOVA with a post-hoc test (Tukey's correction).

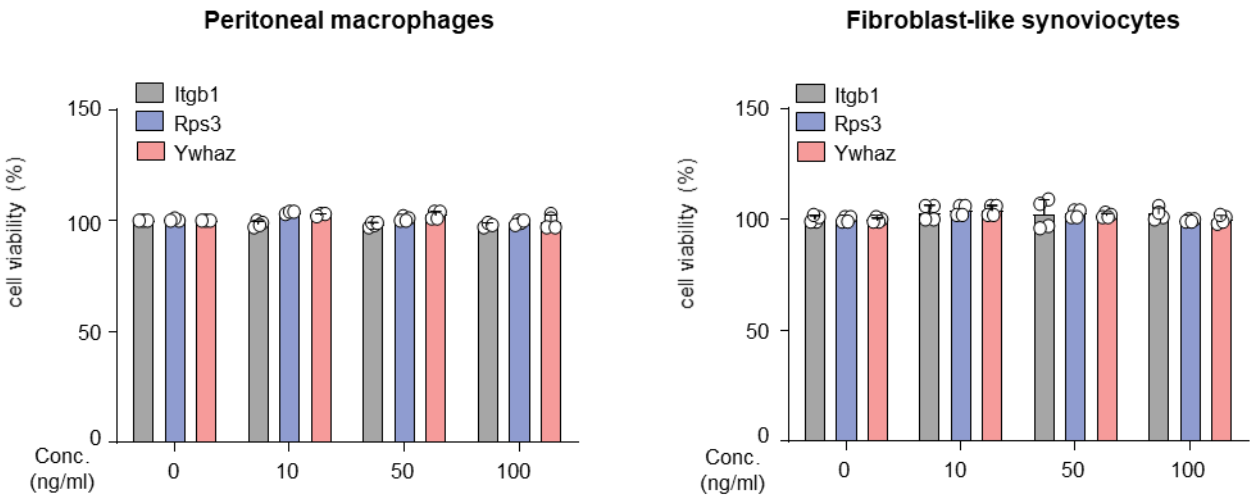

Supplemental Figure 7. No effect of recombinant Itgb1, Rps3, and Ywhaz on the survival of peritoneal macrophages and fibroblast-like synoviocytes (FLSs). Mouse peritoneal macrophages and FLSs were incubated for 12 hours with recombinant Itgb1, Rps3, or Ywhaz protein at multiple concentrations (0, 10, 50, or 100 ng/ml), and their viabilities were determined by MTT assay. Data are the mean ± SD (n=3 to 4).

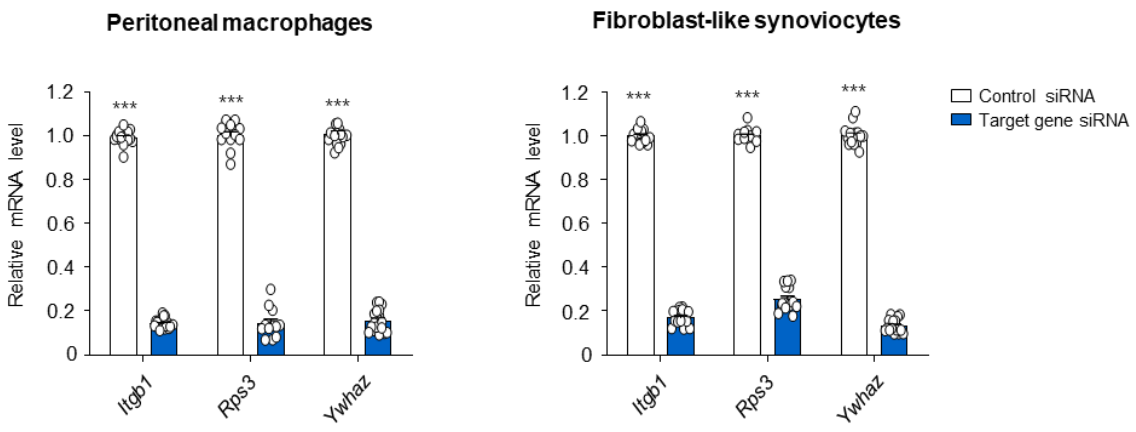

Supplemental Figure 8. Knockdown Validation of Itgb1, Rps3, or Ywhaz. Decrease in mRNA expression levels of *Itgb1*, *Rps3*, and *Ywhaz* in mouse peritoneal macrophages (left) and fibroblast-like synoviocytes (right) transfected for 24 hours with siRNAs against *Itgb1*, *Rps3*, and *Ywhaz*, respectively. The mRNA levels measured by qRT-PCR are first normalized by those of *Gapdh* (internal control) and then further normalized by the mean mRNA expression levels in the cells transfected with control siRNAs. Data obtained from more than three independent experiments in duplicate are shown in the mean ± SEM. ***$p < 0.001$ by Student's *t* test.

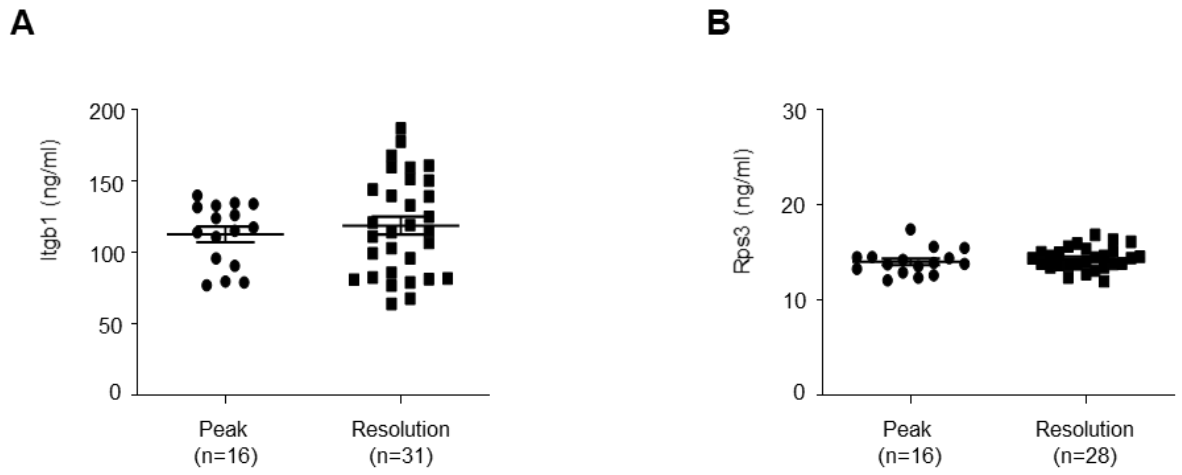

Supplemental Figure 9. No difference in the serum Itgb1 and Rps3 levels between peak and resolution phases of CIA. Levels of Itgb1 (**A**) and Rps3 (**B**) were measured in the sera of CIA mice by ELISA assays at the peak and the resolution phases. Data are the mean ± SEM. The number of mice (*n*) used at each phase is shown.

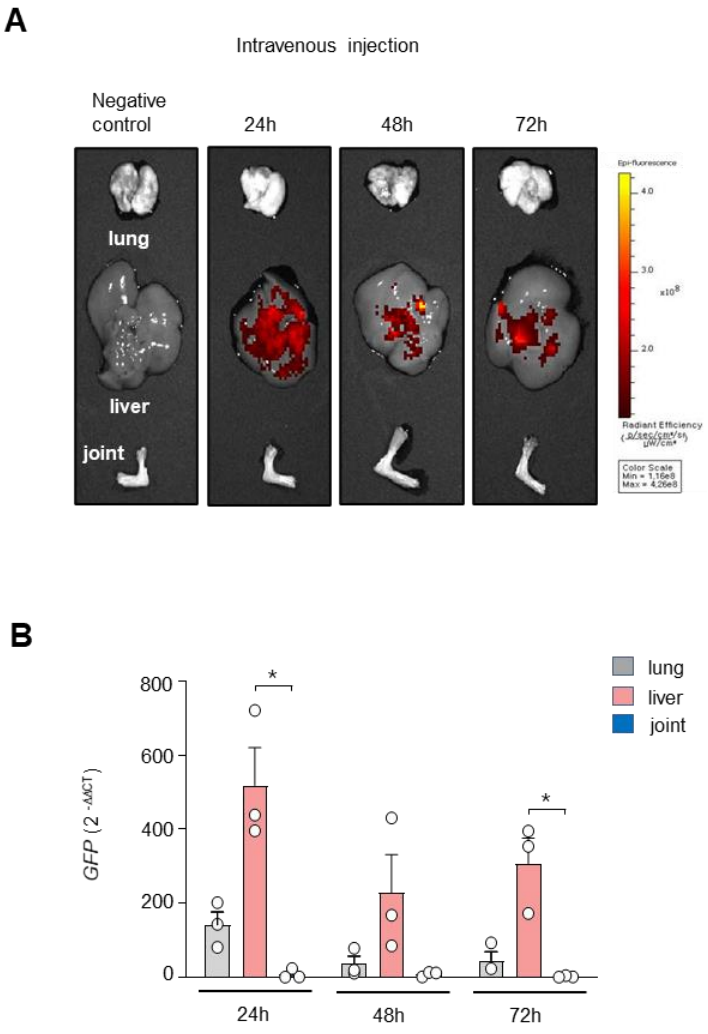

Supplemental Figure 10. GFP expression in the lung, liver, and joints after intra-venous injection of Ad-*Ywhaz*-tagged *GFP* in mice with CIA. (**A** and **B**) GFP imaging (**A**) and qRT-PCR assays for *GFP* (**B**). The lung, liver, and ankle joint of mice with CIA were harvested at 24, 48, and 72 hours after intravenous injection of Ad-*Ywhaz* tagged with *GFP* (at 31, 32, and 33 days after primary immunization, respectively) or those of mice without the injection. For fluorescence imaging, the color bar represents the gradient of radiance efficiency. Representative results from the three mice with similar results are shown in **A**. For qRT-PCR assays, the mRNA expression levels of *GFP* at each time point (n=3 for each time point) are first normalized by those of *Gapdh*, and then further normalized by the mean mRNA expression levels measured in the joint with Ad-*Ywhaz* tagged with *GFP* injection. Data are the mean ± SEM. *$p < 0.05$ as determined by Kruskal-Wallis test with a post-hoc test (Dunn's correction).

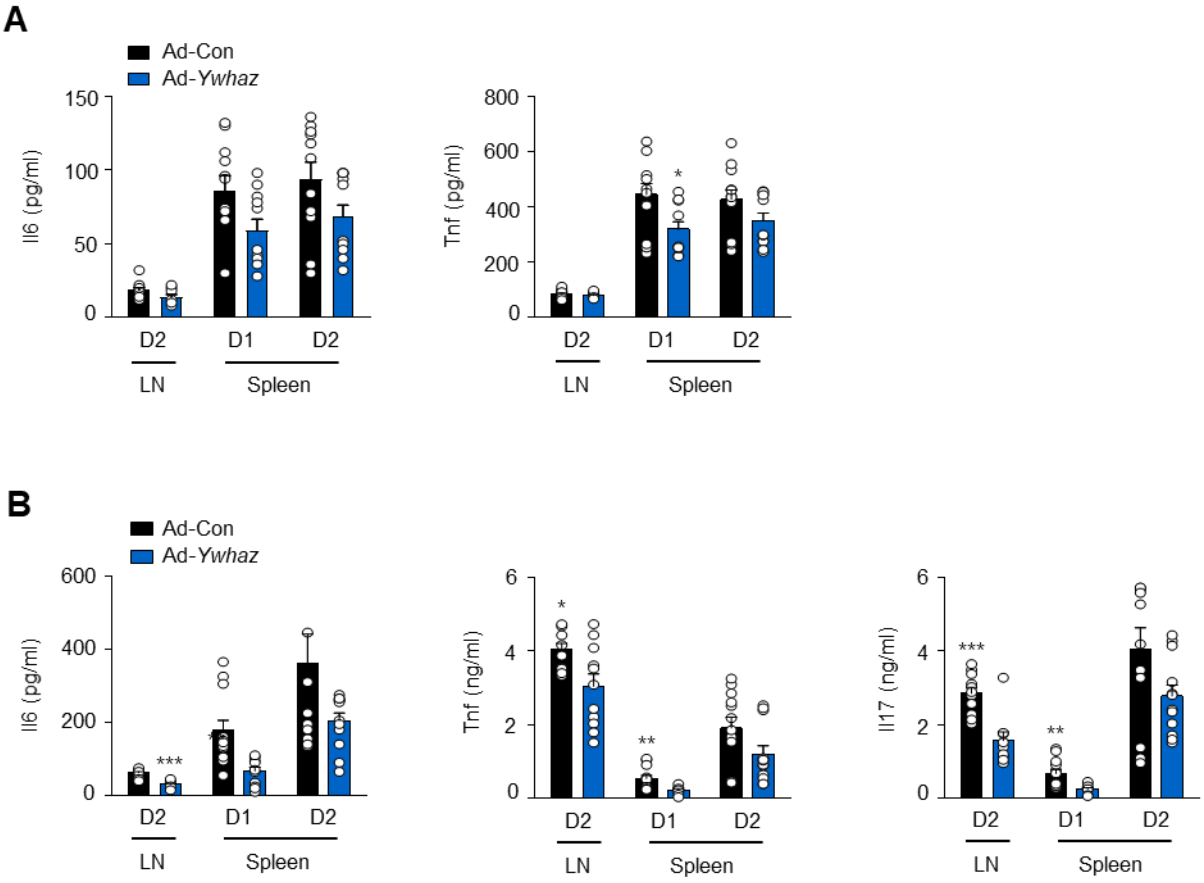

Supplemental Figure 11. Ad-*Ywhaz* suppression of pro-inflammatory cytokine production by lymph node cells and splenocytes of CIA mice. The primary injection of Ad-*Ywhaz* or Ad-Con into CIA mice was performed at 30 days as described in **Figure 7A**. Lymph node and spleen cells were isolated from mice at 33 days (n=4 per group), and then stimulated with 10 ng/ml LPS for an additional one or two days (**A**) or with anti-CD3 plus anti-CD28 Abs (1 μg/ml) for an additional two or four days (**B**). Levels of Il6, Tnf, and Il17 in cell culture supernatants were measured by ELISA assays. Data are the mean ± SEM (n=8). *$p < 0.05$, **$p < 0.01$, and ***$p < 0.001$ as determined by Student's *t* test.

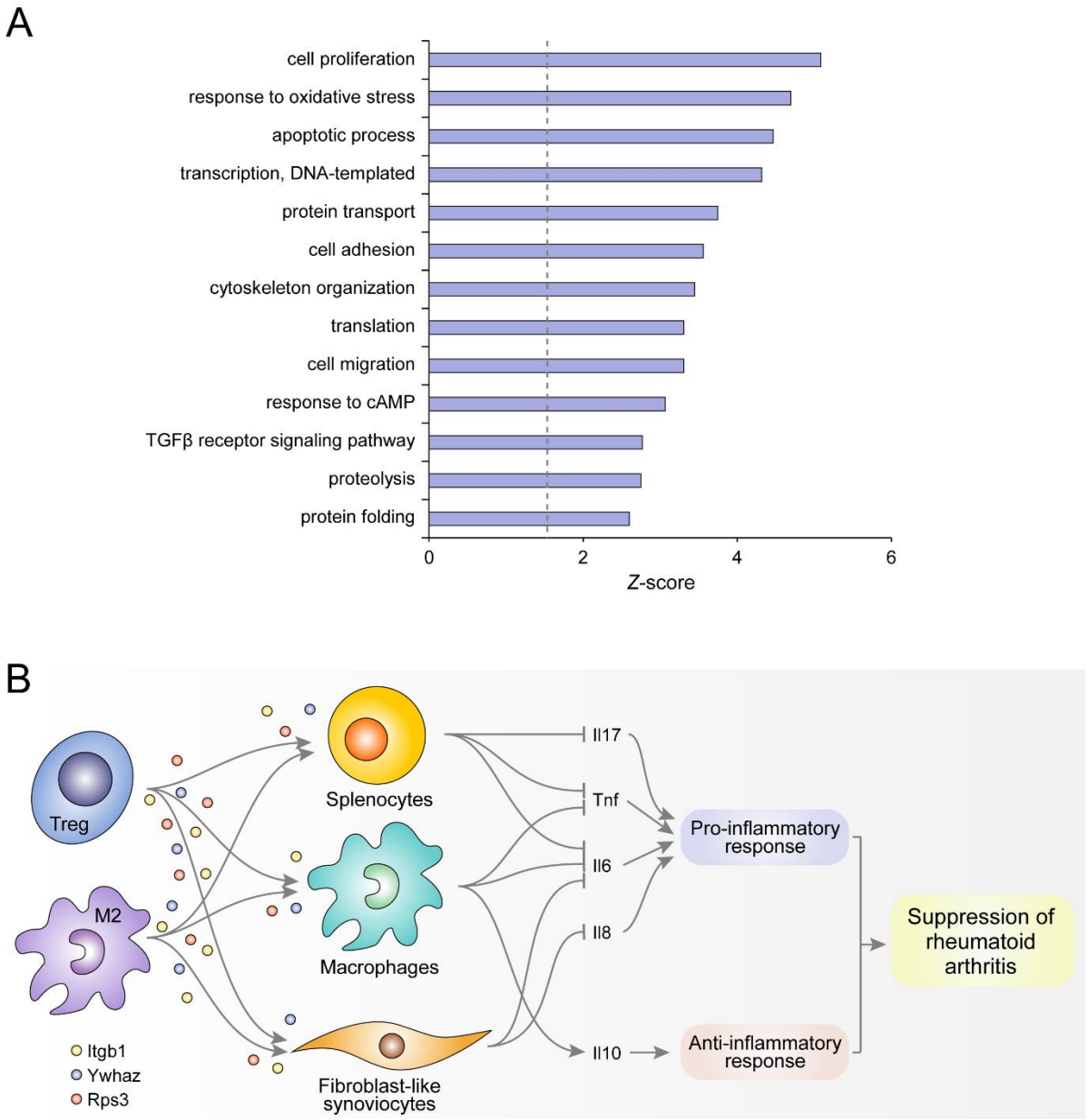

Supplemental Figure 12. Functions of Itgb1, Rps3, and Ywhaz as hub molecules in a molecular network of rheumatoid arthritis. (**A**) Gene ontology biological processes (GOBPs) enriched by the 37 hub-like molecules up-regulated at the resolution phase, compared to at the peak phase. The *Z*-score is defined by $Z=N^{-1}(1-p)$ where $N^{-1}(\cdot)$ is the inverse standard normal distribution and *p* is the enrichment *p* value. The dashed line denotes the cutoff of $p=0.05$. (**B**) Multi-source and multi-target effects of Itgb1, Rps3, and Ywhaz in chronic arthritis. Two major suppressive immune cells (Treg cells and macrophages, left) and three effector cells of RA (splenocytes, macrophages, and fibroblast-like synoviocytes, middle) are displayed in a

molecular network as the source and target cells of the secretory regulators, Itgb1, Rps3, and Ywhaz, at the resolution phase, respectively. Moreover, both increased the release of an anti-inflammatory cytokine, Il10, and decreased the release of pro-inflammatory cytokines (Il6, Il8, Il17 and/or Tnf) by the three secretory regulators are displayed as outputs (right) that lead to the promotion of an anti-inflammatory response and suppression of a pro-inflammatory response during the resolution of arthritis.

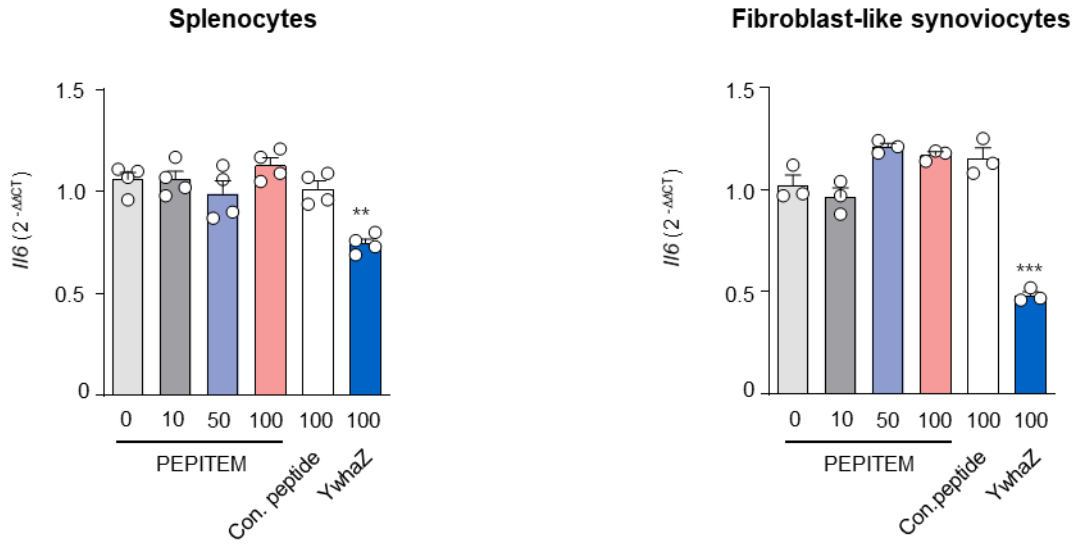

Supplemental Figure 13. Suppression of *Il6* mRNA expression by recombinant Ywhaz is not dependent on a 14-amino acid peptide sequence of Ywhaz, named PEPITEM. Mouse splenocytes (left, n=3) and fibroblast-like synoviocytes (right, n=4) were cultured with multiple concentrations (0, 10, 50, or 100 ng/ml) of PEPITEM peptide, 100 ng/ml of scrambled peptide (Con. peptide), or 100 ng/ml of recombinant Ywhaz protein. The mRNA expression levels of *Il6* are measured by qRT-PCR assays. mRNA levels are first normalized by those of *Gapdh* and then further normalized by the mRNA expression levels of untreated cells. Data are the mean ± SEM. $^{**}p < 0.01$ and $^{***}p < 0.001$ as determined by one-way ANOVA with a post-hoc test (Tukey's correction).

Supplemental References

1. Perretti M, Cooper D, Dalli J, Norling LV. Immune resolution mechanisms in inflammatory arthritis. *Nat Rev Rheumatol.* 2017;13(2):87-99.
2. Ortega-Gomez A, Perretti M, Soehnlein O. Resolution of inflammation: an integrated view. *EMBO Mol Med.* 2013;5(5):661-674.
3. Newman AM, et al. Robust enumeration of cell subsets from tissue expression profiles. *Nat Methods.* 2015;12(5):453-457.
4. Chen Z, Huang A, Sun J, Jiang T, Qin FX, Wu A. Inference of immune cell composition on the expression profiles of mouse tissue. *Sci Rep.* 2017;7:40508.
5. Junker BH, Koschutzki D, Schreiber F. Exploration of biological network centralities with CentiBiN. *BMC Bioinformatics.* 2006;7:219.
6. McInnes IB, Schett G. Cytokines in the pathogenesis of rheumatoid arthritis. *Nature Reviews Immunology.* 2007;7(6):429-442.
7. Farrah T, et al. A high-confidence human plasma proteome reference set with estimated concentrations in PeptideAtlas. *Mol Cell Proteomics.* 2011;10(9):M110 006353.
8. Liu YC, Elly C, Yoshida H, Bonnefoy-Berard N, Altman A. Activation-modulated association of 14-3-3 proteins with Cbl in T cells. *J Biol Chem.* 1996;271(24):14591-14595.
9. Robertson H, Langdon WY, Thien CB, Bowtell DD. A c-Cbl yeast two hybrid screen reveals interactions with 14-3-3 isoforms and cytoskeletal components. *Biochem Biophys Res Commun.* 1997;240(1):46-50.
10. Acuto O, Di Bartolo V, Michel F. Tailoring T-cell receptor signals by proximal negative feedback mechanisms. *Nat Rev Immunol.* 2008;8(9):699-712.

11. Wan F, et al. Ribosomal protein S3: a KH domain subunit in NF-kappaB complexes that mediates selective gene regulation. *Cell.* 2007;131(5):927-939.

12. Baeuerle PA, Henkel T. Function and activation of NF-kappa B in the immune system. *Annu Rev Immunol.* 1994;12:141-179.

13. Ahn EH, et al. Transduced PEP-1-ribosomal protein S3 (rpS3) ameliorates 12-O-tetradecanoylphorbol-13-acetate-induced inflammation in mice. *Toxicology.* 2010;276(3):192-197.

14. Iwata S, Ohashi Y, Kamiguchi K, Morimoto C. Beta 1-integrin-mediated cell signaling in T lymphocytes. *J Dermatol Sci.* 2000;23(2):75-86.

15. Yamada A, Nikaido T, Nojima Y, Schlossman SF, Morimoto C. Activation of human CD4 T lymphocytes. Interaction of fibronectin with VLA-5 receptor on CD4 cells induces the AP-1 transcription factor. *J Immunol.* 1991;146(1):53-56.

16. Yoo SA, et al. Arginine-rich anti-vascular endothelial growth factor (anti-VEGF) hexapeptide inhibits collagen-induced arthritis and VEGF-stimulated productions of TNF-alpha and IL-6 by human monocytes. *J Immunol.* 2005;174(9):5846-5855.

17. Dunning MJ, Smith ML, Ritchie ME, Tavare S. beadarray: R classes and methods for Illumina bead-based data. *Bioinformatics.* 2007;23(16):2183-2184.

18. Bolstad BM, Irizarry RA, Astrand M, Speed TP. A comparison of normalization methods for high density oligonucleotide array data based on variance and bias. *Bioinformatics.* 2003;19(2):185-193.

19. Lee HJ, et al. Direct transfer of alpha-synuclein from neuron to astroglia causes inflammatory responses in synucleinopathies. *J Biol Chem.* 2010;285(12):9262-9272.

20. Hwang D, et al. A data integration methodology for systems biology. *Proc Natl Acad Sci U S A.* 2005;102(48):17296-17301.

21. Huang da W, Sherman BT, Lempicki RA. Systematic and integrative analysis of large gene lists using DAVID bioinformatics resources. *Nat Protoc.* 2009;4(1):44-57.

22. Shannon P, et al. Cytoscape: a software environment for integrated models of biomolecular interaction networks. *Genome Res.* 2003;13(11):2498-2504.

23. Stark C, Breitkreutz BJ, Reguly T, Boucher L, Breitkreutz A, Tyers M. BioGRID: a general repository for interaction datasets. *Nucleic Acids Res.* 2006;34(Database issue):D535-539.

24. Orchard S, et al. The MIntAct project--IntAct as a common curation platform for 11 molecular interaction databases. *Nucleic Acids Res.* 2014;42(Database issue):D358-D363.

25. Licata L, et al. MINT, the molecular interaction database: 2012 update. *Nucleic Acids Res.* 2012;40(Database issue):D857-D861.

26. Salwinski L, Miller CS, Smith AJ, Pettit FK, Bowie JU, Eisenberg D. The Database of Interacting Proteins: 2004 update. *Nucleic Acids Res.* 2004;32(Database issue):D449-D451.

27. Brown KR, Jurisica I. Unequal evolutionary conservation of human protein interactions in interologous networks. *Genome Biol.* 2007;8(5):R95.

28. Blake JA, et al. Mouse Genome Database (MGD)-2017: community knowledge resource for the laboratory mouse. *Nucleic Acids Res.* 2017;45(D1):D723-D729.

29. Kong JS, et al. Anti-neuropilin-1 peptide inhibition of synoviocyte survival, angiogenesis, and experimental arthritis. *Arthritis Rheum.* 2010;62(1):179-190.

30. Flaherty S, Reynolds JM. Mouse Naive CD4+ T Cell Isolation and In vitro Differentiation into T Cell Subsets. *J Vis Exp.* 2015(98).

31. Hunter MM, et al. In vitro-derived alternatively activated macrophages reduce colonic

inflammation in mice. *Gastroenterology.* 2010;138(4):1395-1405.

32. Hardy RS, et al. Characterisation of fibroblast-like synoviocytes from a murine model of joint inflammation. *Arthritis Res Ther.* 2013;15(1):R24.

33. Kong JS, et al. Inhibition of synovial hyperplasia, rheumatoid T cell activation, and experimental arthritis in mice by sulforaphane, a naturally occurring isothiocyanate. *Arthritis Rheum.* 2010;62(1):159-170.

34. Prevoo ML, van 't Hof MA, Kuper HH, van Leeuwen MA, van de Putte LB, van Riel PL. Modified disease activity scores that include twenty-eight-joint counts. Development and validation in a prospective longitudinal study of patients with rheumatoid arthritis. *Arthritis Rheum.* 1995;38(1):44-48.

35. van Gestel AM, Prevoo ML, van 't Hof MA, van Rijswijk MH, van de Putte LB, van Riel PL. Development and validation of the European League Against Rheumatism response criteria for rheumatoid arthritis. Comparison with the preliminary American College of Rheumatology and the World Health Organization/International League Against Rheumatism Criteria. *Arthritis Rheum.* 1996;39(1):34-40.

36. Chimen M, et al. Homeostatic regulation of T cell trafficking by a B cell-derived peptide is impaired in autoimmune and chronic inflammatory disease. *Nat Med.* 2015;21(5):467-475.

37. Cohen J. *Statistical Power Analysis for the Behavioral Sciences, 2nd Edition.* Hillsdale, New Jersey, USA: Lawrence Erlbaum Associates; 1988.

38. Alarcon B, Berkhout B, Breitmeyer J, Terhorst C. Assembly of the human T cell receptor-CD3 complex takes place in the endoplasmic reticulum and involves intermediary complexes between the CD3-gamma.delta.epsilon core and single T cell receptor alpha or beta chains. *J Biol Chem.* 1988;263(6):2953-2961.

39. Stubbington MJ, et al. An atlas of mouse CD4(+) T cell transcriptomes. *Biol Direct.* 2015;10:14.

40. Qin X, et al. Regulation of Th1 and Th17 cell differentiation and amelioration of experimental autoimmune encephalomyelitis by natural product compound berberine. *J Immunol.* 2010;185(3):1855-1863.

41. Nakamura S, et al. Expression and responsiveness of human interleukin-18 receptor (IL-18R) on hematopoietic cell lines. *Leukemia.* 2000;14(6):1052-1059.

42. Annunziato F, Cosmi L, Liotta F, Maggi E, Romagnani S. The phenotype of human Th17 cells and their precursors, the cytokines that mediate their differentiation and the role of Th17 cells in inflammation. *Int Immunol.* 2008;20(11):1361-1368.

43. Halvorsen EC, et al. Maraviroc decreases CCL8-mediated migration of CCR5(+) regulatory T cells and reduces metastatic tumor growth in the lungs. *Oncoimmunology.* 2016;5(6):e1150398.

44. Holt MP, Punkosdy GA, Glass DD, Shevach EM. TCR Signaling and CD28/CTLA-4 Signaling Cooperatively Modulate T Regulatory Cell Homeostasis. *J Immunol.* 2017;198(4):1503-1511.

45. Corthay A. How do regulatory T cells work? *Scand J Immunol.* 2009;70(4):326-36.

46. Josefowicz SZ, Lu LF, Rudensky AY. Regulatory T cells: mechanisms of differentiation and function. *Annu Rev Immunol.* 2012;30:531-564.

47. Vocanson M, et al. Inducible costimulator (ICOS) is a marker for highly suppressive antigen-specific T cells sharing features of TH17/TH1 and regulatory T cells. *J Allergy Clin Immunol.* 2010;126(2):280-9, 9 e1-7.

48. Anz D, et al. CD103 is a hallmark of tumor-infiltrating regulatory T cells. *Int J Cancer.* 2011;129(10):2417-2426.

49. Lai L, Alaverdi N, Maltais L, Morse HC, 3rd. Mouse cell surface antigens: nomenclature and immunophenotyping. *J Immunol.* 1998;160(8):3861-3868.

50. Campana D, et al. Human B cell development. I. Phenotypic differences of B lymphocytes in the bone marrow and peripheral lymphoid tissue. *J Immunol.* 1985;134(3):1524-1530.

51. Paulie S, et al. The human B lymphocyte and carcinoma antigen, CDw40, is a phosphoprotein involved in growth signal transduction. *J Immunol.* 1989;142(2):590-595.

52. Chu PG, Arber DA. CD79: a review. *Appl Immunohistochem Mol Morphol.* 2001;9(2):97-106.

53. Boross P, Leusen JH. Mechanisms of action of CD20 antibodies. *Am J Cancer Res.* 2012;2(6):676-690.

54. Coxon A, et al. Fc gamma RIII mediates neutrophil recruitment to immune complexes. a mechanism for neutrophil accumulation in immune-mediated inflammation. *Immunity.* 2001;14(6):693-704.

55. Cowland JB, Borregaard N. Molecular characterization and pattern of tissue expression of the gene for neutrophil gelatinase-associated lipocalin from humans. *Genomics.* 1997;45(1):17-23.

56. Birgens HS. Lactoferrin in plasma measured by an ELISA technique: evidence that plasma lactoferrin is an indicator of neutrophil turnover and bone marrow activity in acute leukaemia. *Scand J Haematol.* 1985;34(4):326-331.

57. Newton RA, Hogg N. The human S100 protein MRP-14 is a novel activator of the beta 2 integrin Mac-1 on neutrophils. *J Immunol.* 1998;160(3):1427-1435.

58. Smith MJ, Koch GL. Differential expression of murine macrophage surface

glycoprotein antigens in intracellular membranes. *J Cell Sci.* 1987;87 (Pt 1):113-119.

59. Kadl A, et al. Identification of a novel macrophage phenotype that develops in response to atherogenic phospholipids via Nrf2. *Circ Res.* 2010;107(6):737-746.

60. Buhling F, et al. Cathepsin K--a marker of macrophage differentiation? *J Pathol.* 2001;195(3):375-382.

61. Gautier EL, et al. Gene-expression profiles and transcriptional regulatory pathways that underlie the identity and diversity of mouse tissue macrophages. *Nat Immunol.* 2012;13(11):1118-1128.

62. Jablonski KA, et al. Novel Markers to Delineate Murine M1 and M2 Macrophages. *PLoS One.* 2015;10(12):e0145342.

63. Beyer M, et al. High-resolution transcriptome of human macrophages. *PLoS One.* 2012;7(9):e45466.

64. Asano K, et al. Intestinal CD169(+) macrophages initiate mucosal inflammation by secreting CCL8 that recruits inflammatory monocytes. *Nat Commun.* 2015;6:7802.

65. Landmann R, Muller B, Zimmerli W. CD14, new aspects of ligand and signal diversity. *Microbes Infect.* 2000;2(3):295-304.

66. Cannarile MA, Weisser M, Jacob W, Jegg AM, Ries CH, Ruttinger D. Colony-stimulating factor 1 receptor (CSF1R) inhibitors in cancer therapy. *J Immunother Cancer.* 2017;5(1):53.

67. Farber JM. A macrophage mRNA selectively induced by gamma-interferon encodes a member of the platelet factor 4 family of cytokines. *Proc Natl Acad Sci U S A.* 1990;87(14):5238-5242.

68. Furukawa S, et al. Interleukin-33 produced by M2 macrophages and other immune cells contributes to Th2 immune reaction of IgG4-related disease. *Sci Rep.* 2017;7:42413.

69. Liao X, et al. Kruppel-like factor 4 regulates macrophage polarization. *J Clin Invest.* 2011;121(7):2736-2749.

70. Keshav S, Chung P, Milon G, Gordon S. Lysozyme is an inducible marker of macrophage activation in murine tissues as demonstrated by in situ hybridization. *J Exp Med.* 1991;174(5):1049-1058.